HHS Public Access

Author manuscript

Acta Biomater. Author manuscript; available in PMC 2020 May 01.

Published in final edited form as:

Acta Biomater. 2019 May ; 90: 300–313. doi:10.1016/j.actbio.2019.03.048.

Dual Functional Immunostimulatory Polymeric Prodrug Carrier with Pendent Indoximod for Enhanced Cancer Immunochemotherapy

Zhuoya Wan[1,2], **Jingjing Sun**[1,2], **Jieni Xu**[1,2], **Pearl Moharil**[1,2], **Jing Chen**[1,2], **Junchi Xu**[3], **Junjie Zhu**[1,2], **Jiang Li**[1,2], **Yixian Huang**[1,2], **Pengfei Xu**[1,2], **Xiaochao Ma**[1,2], **Wen Xie**[1,2], **Binfeng Lu**[3], and **Song Li**[*,1,2]

[1)]Center for Pharmacogenetics, School of Pharmacy, University of Pittsburgh, Pittsburgh, Pennsylvania 15261, USA.

[2)]Department of Pharmaceutical Sciences, School of Pharmacy, University of Pittsburgh, Pittsburgh, Pennsylvania 15261, USA.

[3)]Department of Immunology, School of Medicine, University of Pittsburgh, Pittsburgh, Pennsylvania 15261, USA.

Abstract

Immunotherapy based on checkpoint blockade has been regarded as one of the most promising approaches towards many types of cancers. However, low response rate hinders its application due to insufficient tumor immunogenicity and immunosuppressive tumor microenvironment. To achieve an overall enhanced therapeutic outcome, we developed a dual-functional immunostimulatory polymeric prodrug carrier modified with pendent indoximod, an indoleamine 2,3-dioxygenase (IDO) inhibitor that can be used to reverse immune suppression, for co-delivery of Doxorubicin (Dox), a hydrophobic anticancer agent that can promote immunogenic cell death (ICD) and elicit antitumor immunity. The resulted carrier denoted as POEG-b-PVBIND, consisting of poly (oligo (ethylene glycol) methacrylate) (POEG) hydrophilic blocks and indoximod conjugated hydrophobic blocks, is rationally designed to improve immunotherapy by synergistically modulating the tumor microenvironment (TME). Our data showed that Dox-triggered ICD promoted intra-tumoral infiltration of $CD8^+$ T cells and IFN-γ-production by $CD8^+$ T cells. Meanwhile, cleaved indoximod significantly increased $CD8^+$ T cell infiltration while reducing the immunosuppressive T regulatory cells (Tregs). More importantly, Dox/POEG-b-PVBIND micelles led to significantly improved tumor regression in an orthotopic murine breast cancer model compared to both Dox-loaded POEG-b-PVB micelles (a control inert carrier) and POEG-b-PVBIND micelles alone, confirming combination effect of indoximod and Dox in improving the overall antitumor activity.

[*]Corresponding Authors: Song Li, Professor, Sol4@pitt.edu (S. Li).

Graphical Abstract

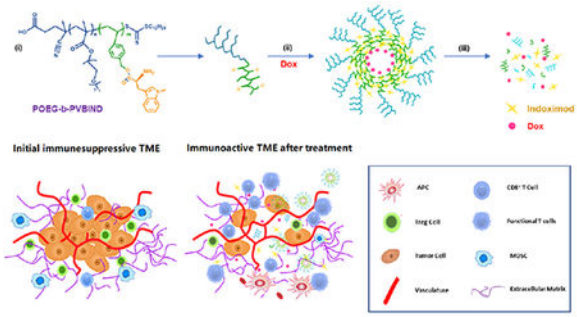

Keywords

Indoximod; Immunochemotherapy; Indoleamine 2,3-dioxygenase; Immuno-oncology

1. Introduction

Immunotherapy has been regarded as one of the most promising approaches towards many types of cancers, especially with the success of Yevoy® and Opdivo® that target CTLA-4 and PD-1, respectively[1–4]. Indoleamine 2,3-dioxygenase (IDO) has emerged as another important immuno-oncology target for next groups of immune-based drugs due to its important role in driving the immune suppressive TME through tryptophan depletion and kynurenine accumulation[5–6]. Five mechanistically distinct IDO inhibitors were under development over the past few years[7]. But low clinical response rates hinder their application. Combination with chemotherapy is one of the validated strategies to significantly improve anti-tumor response compared to each single agent alone[8–10]. The mechanism of action (MOA) behind this successful combination is largely due to an overall enhanced immune response, since IDO inhibitors could potentially amplify the immune response induced by the chemo-therapeutic agents that can trigger the immunogenic cell death (ICD)[11–14]. However, highly efficient combination therapy was limited by poor solubility, different pharmacokinetic profiles, poor tumor biodistribution and systemic toxicities of these combined agents[15].

Polymers with customizable structures have been widely exploited as ideal delivery carriers for combination therapy. Specifically, polymeric micelles have shown great clinical potential due to their capability of co-encapsulating poorly soluble drugs and efficiently delivering them into tumor areas via EPR effect[15]. Prodrug polymers can also be designed to serve as dual-functional micelle carriers to co-deliver other hydrophobic drugs for combination effect[16–17]. Significantly enhanced antitumor effect was achieved recently based on a PEG_{2k}-modified prodrug of NLG-919 for co-delivery of paclitaxel, an ICD-inducing agent, and NLG919, a selective IDO1 inhibitor. More importantly, therapeutic advantages were also observed in comparison with combination of Abraxane and i.v. delivery of NLG919 via an inert nanocarrier as well as combination of Abraxane and oral delivery of NLG919, indicating highly efficient immunochemotherapy based on this strategy[18]. However, a major

limitation for the NLG-919-paclitaxel system is the low loading capacity of NLG919, because each molecule of nanocarrier carries only one molecule of NLG919.

There are two isoforms of the IDO enzymes, IDO1 and IDO2[19]. In addition, tryptophan-2,3-dioxygenase (TDO) is also involved in tryptophan metabolism[20]. Among them, IDO1 has been most extensively studied because IDO1 is overexpressed in many types of tumor cells as well as certain immune cells in tumor tissues[21]. Surprisingly, selective IDO1 inhibitors such as NLG-919 failed in clinical trials. It is unclear whether delivery is an issue or other issues are involved in the unexpected failure. Indoximod (IND) was another well-studied IDO inhibitor. Recent studies have demonstrated that IND not only acted in inhibiting the IDO activity but also drove antitumor immune responses independently from IDO/TDO. In the presence of IND, the activity of IDO in dendritic cells (DCs) is inhibited. Meanwhile, IND promotes T cells activation and proliferation and reprograms Treg cells into T helper cells in an IDO/TDO independent manner[22]. Additionally, IND can prevent the recruitment of myeloid-derived suppressor cells (MDSCs) in the tumor site[7, 22–25]. Therefore, IND is able to exert multiple immunomodulatory effects in tumors[5, 19, 22–23, 26–28]. Therapeutic benefits were also demonstrated in the clinic with IND in combination with other treatments such as chemotherapy or anti-PD-1 antibody[29–34].

Despite the demonstrated potential, the pharmaceutical utility of IND is limited by its poor water solubility and low bioavailability and various IND derivatives of improved solubility and PK profile have been developed[35]. One such prodrug, NLG-802, is currently being tested in clinic in patients with advanced solid tumors[36–37]. Another strategy to improve the therapeutic efficacy focuses on the development of a nanocarrier to enhance delivery of IND to tumors. Several IND-based nanomedicines have been reported including an oral nanocrystal formulation for lung cancer[35], an intratumorally injectable liposome for co-delivery of IND and hydrophilic drugs for pancreatic cancer[38], and an intratumorally injectable IND hydrogel in combination with PD1 antibody for treating melanoma[39]. However, few reports have been published on systemic co-delivery of IND and hydrophobic chemotherapeutic agents. In addition, it is difficult to achieve an optimal release of IND and chemodrug in a temporal and spatial manner[40].

Based on our success and limitation of NLG919-based prodrug carrier, we designed and synthesized an IND-based prodrug polymer, POEG-b-PVBIND, which could self-assemble to form micelles and serve as a dual-functional carrier to deliver Dox, a DNA-damaging agent that can promote ICD (Scheme 1, Figure S1). POEG-b-PVBIND consists of hydrophilic segments of poly (oligo (ethylene glycol) methacrylate) (POEG) and hydrophobic segments of vinylbenzyl chloride with a number of IND molecules covalently attached. These two segments were polymerized in a tunable manner via reversible addition fragmentation chain transfer (RAFT) polymerization for optimal codelivery of IND and DOX. We hypothesize that the physically loaded Dox will be rapidly released from the nanocarrier at the tumor site, leading to ICD of tumor cells and the induction of antitumor immunity. Meanwhile, the covalently conjugated IND will be slowly released, helping to sustain an active immune microenvironment for an extended period of time. Using a 4T1.2 murine breast cancer model, we demonstrated that intravenous administration of POEG-b-PVBIND micelles alone was effective in enhancing immune responses and exhibited

antitumor activity in vivo. More importantly, delivery of Dox via POEG-b-PVBIND micelles led to potent and sustained antitumor effect, with improved tumor immune microenvironment.

2. Materials and Method

2.1 Materials

Indoximod (IND) was purchased from Sigma-Aldrich (MO, USA). Doxorubicin hydrochloride (DOX·HCl) was obtained from LC Laboratories (MA, USA). Vinylbenzyl chloride, potassium carbonate (K_2CO_3), azobisisobutyronitrile (AIBN), petroleum ether (PE), sodium hydroxide (NaOH), 2-hydroxyethyl methacrylate, di-tert-butyl dicarbonate, 1,4-dioxane, dimethylformamide (DMF), dimethyl sulfoxide (DMSO), tetrahydrofuran (THF), triethylamine (TEA), 4-cyano-4-[(dodecylsulfanylthiocarbonyl) sulfanyl] pentanoic acid, poly(ethylene glycol) methyl ether methacrylate (OEGMA, Mn=500), and 1,1'-dioctadecyl-3,3,3',3'-tetramethylindotricarbocyanine iodide (DiR) were purchased from Fisher Scientific (Pittsburgh, PA).

2.2 Cell lines and tumor models

4T1.2 (murine breast cancer cell line) cells were obtained from ATCC (Manassas, VA) and cultured in Dulbecco's Modified Eagle's Medium (DMEM) supplemented with 10% fetal bovine serum (FBS) and 1% penicillin-streptomycin at 37 °C in a humidified environment with 5% CO_2[41].

The female BALB/c mice (4–5 weeks) of 18–20 g were purchased from Charles River (Davis, CA, USA). All animal protocols were approved by Animal Use and Care Administrative Advisory Committee at the University of Pittsburgh and all animal studies were performed according to the guidelines approved by the Ethics Committee of University of Pittsburgh. All the mice were housed under pathogen free conditions. Orthotopic 4T1 breast tumors were generated by injecting 5×10^5 cells into the mammary fat pad (left) of female BALB/c mice at the age of 6–8 weeks.

2.3 Synthesis of Boc-Protected Indoximod

IND (200mg, 0.909mmol, 1.0 eq), NaOH (86mg, 2.15mmol, 2.36 eq) and di-tert-butyl dicarbonate (470mg, 2.15mmol, 2.36eq) were dissolved in a mixed solvent of THF (9ml) and H_2O (9.8ml). The mixture was stirred at room temperature for 48h. THF was evaporated under reduced pressure, and the remaining aqueous layer was acidified with 1N HCl to pH=3. IND-Boc was extracted by ethylacetate three times, and the organic layer was collected and concentrated to give the product as a yellow solid (264mg, 0.825mmol, 90% yield)[42].

2.4 Synthesis of POEG-MacroCTA

POEG MacroCTA was synthesized and purified following a published protocol[16]. Briefly, OEGMA 500 (3.05g, 6.10mmol, 20.5 eq), 4-Cyano-4-[(dodecylsulfanylthiocarbonyl)sulfanyl] pentanoic acid (120mg, 0.297 mmol, 1.0 eq), AIBN (8mg, 0.048mmol) and 5ml anhydrous THF were mixed in a Schlenk tube. The mixture was

then purged with nitrogen so as to remove the oxygen dissolved in the reaction solvent by using a freeze-pump-thawing method. Then, the tube was immersed in an oil bath at 85°C for 130 mins under nitrogen protection. After polymerization, the reaction was first quenched in a liquid nitrogen bath. Next, the POEG MacroCTA was purified by precipitation and extraction using cold diethyl ether three times. Finally, POEG MacroCTA was obtained in the form of yellow liquid oil (2.3977g, 91% yield), followed by vacuum drying. The conversion rate was 86% as determined by ^{1}H NMR spectroscopy of POEG MacroCTA before purification, which was equivalent to 17 POEG units.

2.5 Synthesis of POEG-b-PVB and POEG-b-PVBIND Polymers

POEG MacroCTA (213mg, 0.025mmol, 1.0 eq), vinylbenzyl chloride (70mg, 0.45mmol, 18.0 eq), AIBN (2mg, 0.0122mmol), and 2.5ml anhydrous 1,4-Dioxane were added into a Schlenk tube. The mixture was de-oxygenated three times using a free-pump-thaw method. Then the tube was immersed in an oil bath at 90°C for 5.5 hours. At the completion of reaction, the mixture was precipitated in petroleum ether three times. The POEG-b-PVB polymer was finally obtained after vacuum drying.

To obtain POEG-b-PVBIND polymer, the as-synthesized POEG-b-PVB polymer (200mg, 0.018mmol, 1.0 eq), Boc-Protected IND (250mg, 0.78mmol, 43.3 eq), and K_2CO_3 (181mg, 1.31mmol, 72.7 eq) were dissolved in 5.5ml DMF for further reaction. One molecule of POEG-b-PVB polymer has ten benzyl chloride units (Figure 1A) and the input of benzyl chloride was 0.18 mmol. The input of Boc-Protected IND was calculated to be 0.78 mmol. Therefore, the reaction ratio of IND/benzyl chloride was 4.3. After stirring at 80°C overnight, 5ml cool water was added into reaction mixture and the mixture was then dialyzed (3500 Da MW cutoff) against DMSO for one day and deionized water for another two days. The final product POEG-b-PVBIND-Boc was obtained after lyophilization. The POEG-b-PVBIND-Boc polymer was deprotected in a mixture solution of DCM/TFA (6/5, v/v) at ambient temperature. After 75 min, the reaction mixture was precipitated in diethyl ether. The crude product was dissolved in the mixed solvents of DCM/ethanol and was then precipitated by ether again. The deprotected POEG-b-PVBIND polymer was dried in vacuum to afford the product in a sticky and brown oil form.

2.6 Micelle Preparation and Characterization

To obtain Dox free base solution, 10mg Dox hydrochloride and 15uL TEA were added into 1 ml DMSO for overnight reaction[16, 43–45]. The POEG-b-PVBIND blank micelles and Dox-loaded POEG-b-PVBIND micelles were prepared through a dialysis method. In brief, 25 mg POEG-b-PVBIND polymer was dissolved in 400μL DMSO. Dox free base/DMSO stock solution (70μL) at a concentration of 10mg/ml was added into this polymer solution (DOX/polymer:1/35, w/w). After a 60s mixing, the mixture was placed into a dialysis bag (3500 Da MW cutoff) and dialyzed against 1× PBS buffer overnight so as to remove organic solvent and free Dox. Blank micelles were prepared in a similar method without adding Dox solution.

The size distribution and zeta potential of Dox-loaded POEG-b-PVBIND micelles and POEG-b-PVBIND micelles were examined by a Zeta Nanosizer (Malvern) after a 0.45μm

filtration. All the sizes of micelles were presented using diameter. The morphology of micelles was confirmed by transmission electron microscopy (TEM) using a negative staining method.

The Dox concentration was detected by a Waters 2475 Fluorescence Detector (excitation 490 nm/emission 600 nm). The Dox Loading Efficiency (DLE) and Dox Loading Capacity (DLC) were calculated as the following equations:

$$\text{DLE}(\%) = (\text{Weight of Loaded Drug} / \text{Weight of Input Drug}) \times 100$$

$$\text{DLC}(\%) = (\text{Weight of Drug Loaded} / \text{Weight of Polymer} + \text{Weight of input Drug}) \times 100$$

2.7 Critical Micelle Concentration (CMC) and Storage Stability

The CMC value of POEG-b-PVBIND micelles was determined using nile red as a fluorescence probe. In brief, equal aliquots of nile red DCM solution (photo-sensitive) were added to test tubes and DCM solvent was evaporated by air flow followed by further drying by vacuum pump. A series of concentrations of POEG-b-PVBIND micelles ranging from 0.5 mg/ml to 1.0×10^{-4} mg/ml, were then added into those test tubes for overnight incubation in a dark place. The final concentration of nile red was kept at 6.0×10^{-7} mol/L after dilution. The fluorescence was determined by a Waters 2475 Fluorescence Detector (excitation 550 nm/emission 520/720 nm). The CMC value was determined as the cross-point when extrapolating the intensity at low and high concentration regions. The colloidal stability of POEG-b-PVBIND and POEG-b-PVBIND/Dox was evaluated by following the changes in particle sizes and drug content during storage at 4 °C.

2.8 In Vitro Cytotoxicity of POEG-b-PVBIND micelles

The in vitro cytotoxicity of free Dox, POEG-b-PVBIND alone, POEG-b-PVBIND/Dox, and POEG-b-PVB/Dox against 4T1.2 was evaluated and compared by MTT assay. 4T1.2 at 2500 cells/well were seeded in a 96-well plate. After 12 hours of incubation, cell culture medium was removed and a series of concentrations of free Dox, POEG-b-PVBIND, POEG-b-PVBIND/Dox and POEG-b-PVB/Dox were added to the cells. After 48h incubation, the medium was replaced with 100 uL 1× MTT solution for four-hour incubation. Then, the medium was completely removed and MTT crystals were solubilized by 100uL DMSO in each well. Absorbance was determined by a micro-plate reader at wavelength of 550nm. Untreated cells were used as a positive control. Cell viability was calculated as $((OD_{treated} - OD_{blank}) \times 100\%)$.

2.9 In Vitro Drug Release

To study the stability and release profile of POEG-b-PVBIND/Dox under physiological conditions, in vitro release rate of Dox from POEG-b-PVBIND/Dox at pH 7.4 was evaluated using a dialysis method. PBS buffer solution (0.1 M) containing 0.5% (w/v) Tween 80 was prepared so as to solubilize Dox base. Briefly, 300 μL of POEG-b-PVBIND/Dox and Dox Hydrochloride containing 0.15 mg Dox were placed into dialysis bags (MWCO 3.5 kDa), immersed into 50 mL capped tubes and dialyzed against 40mL PBS. This experiment was

performed in a 37 °C incubation shaker at a speed of 100 rpm. At each predetermined time intervals, an aliquot (2 mL, 37°C) was drawn from the dialysate and was replenished with the same amount of fresh medium. The released Dox from those micelles was measured by fluorescence spectrometry. A standard curve was generated with Dox of the following concentrations: 1.25ug/ml, 0.9375ug/ml, 0.625ug/ml, 0.46875ug/ml, 0.3125ug/ml, 0.234375ug/ml, 0.15625ug/ml, 0.1171875ug/ml, and 0.078125ug/ml. R^2 (≈1) indicates that the regression predictions perfectly fit the data within these gradient concentrations (Figure S2).

The release of IND from POEG-b-PVBIND was also examined at different times in presence of porcine liver esterase (50 U/ml, Sigma-Aldrich, USA). The released IND was derivatized with 6-aminoquinolyl-n-hydroxysuccinimidyl carbamate and measured by UPLC-QTOFMS.[46]

2.10 In Vivo Distribution Profile

To investigate the distribution profile of POEG-b-PVBIND micelles in vivo, 1×10^7 4T1.2 cells were inoculated in the mammary gland of BALB/c mice. Ten days later, the mice bearing 4T1.2 tumors of ~200 mm^3 were intravenously injected with free 1,1'-Dioctadecyl-3,3,3',3'-Tetramethylindotricarbocyanine Iodide (DiR) or DiR-loaded POEG-b-PVBIND at a DiR dose 5.0 mg/kg. The mice were sacrificed at 2h, 4h, 12h, 24h, and 36h post-injection. Near-infrared fluorescence imaging in vivo was carried out with an IVIS imaging system. The tumors and major organs were then collected for ex vivo imaging.

To further investigate Dox delivery efficiency of POEG-b-PVBIND micelles, groups of five BALB/c mice bearing 4T1.2 tumors of ~200 mm^3 were i.v. administered with free Dox, POEG-b-PVB/Dox and POEG-b-PVBIND/Dox at a dose of 5 mg Dox per kg. Mice were sacrificed 24 hours after injection and tumor tissues were collected[47]. Tumor frozen sections were obtained and then the fluorescence images were collected by CLSM (Ziss 710).

2.11 Anti-tumor Efficacy Study

Twenty-five female BALB/c mice (4–5 weeks) were used in this experiment and each mouse was s.c inoculated with 4T1.2 cells (2×10^5 cells/mouse)[48]. Mice were randomly divided into five groups (n=5) after tumor sizes reached around 30 mm^3. Free Dox, POEG-b-PVBIND micelles, POEG-b-PVBIND/Dox and POEG-b-PVB/Dox were intravenously injected into each group at a Dox does of 5mg/kg on days 0, 3 and 6, respectively. Tumor volumes were measured and calculated every three days based on the formula: $(L \times W^2)/2$ (L = Longest diameter; W = Shortest diameter)[49]. Data were presented as relative tumor volume (tumor volume at a given time point / initial tumor volume before 1st injection).

After completion of this therapeutic efficacy study on day 19, mice were sacrificed and tumor tissues and major organs were collected. The excised tumors were weighted separately and the inhibition ratio (IR) was calculated as IR (%) = $[(W_c - W_t) / W_c] \times 100$. The W_c and W_t represent tumor weights for control group and each treatment group, respectively.

To further evaluate the anti-tumor efficacy of POEG-b-PVBIND/Dox and POEG-b-PVBIND micelles, tumors in each group were fixed in PBS solution containing 10% paraformaldehyde and sectioned into 4 um slices. Tumor sections were stained with hematoxylin and eosin (H&E) for histopathological evaluation using a Zeiss Axiostar plus Microscope. Immunohistochemical analysis (IHC) of Ki67 protein was carried out using the labeled streptavidin-biotin method. Ki67 expression was quantified by calculating the number of Ki-67 positive cells/total number of cells in five randomly selected areas.

2.12 Quantification of Tumor-Infiltrating Lymphocytes

Tumor-infiltrating lymphocytes with various treatments were analyzed by flow cytometry. Female BALB/c mice bearing 4T1.2 tumor (~30 mm^3) were treated with free Dox, POEG-b-PVBIND, POEG-b-PVBIND/Dox micelles and POEG-b-PVB/Dox once every 3 days at a DOX dose of 5 mg/kg. Tumors were harvested and dipped into 1mL RPMI medium on ice one day following the last treatment. The tissues were cut into small pieces with scissors and 300–500ul Lysas Enzyme and 2ul DNAse were added. Following a 30 min incubation, tumor pieces were further grinded into suspension with cover glass and were filtered using 100um Nylon Mash. Single cell suspensions were prepared and multi-parameter staining was used to identify the immune cell populations as followings: (i) $CD8^+$ T cells ($CD45^+$ $CD8^+$) and $CD4^+$ T cells ($CD45^+$ $CD4^+$); (ii) Tregs ($CD45^+$ $CD4^+$ $Foxp3^+$); (iii) Macrophage M1 type ($CD11b^+$, $F4/80^+$, $CD206^-$) and Macrophage M2 type ($CD45^+$ $CD11b^+$, $F4/80^+$, $CD206^+$); and (iv) MDSC ($CD45^+$, $CD11b^+$, $Gr\text{-}1^+$).

2.13 Safety Evaluation

To examine the potential toxicity of different treatments, weight changes throughout the in vivo experiments were monitored. In addition, serum and major organs were collected at the completion of the therapy experiment[50]. The organs were fixed with 4% (v/v) paraformaldehyde in PBS (pH 7.4), embedded in paraffin, and sectioned into 4 um slices[49]. Each section was processed for H&E staining and observed under a Zeiss Axiostar plus Microscope[51]. In addition, several biological markers for liver/kidney function were examined from the serum samples including alanine transaminase (ALT), aspartate transaminase (AST), alkaline phosphatase (ALP), blood urea nitrogen (BUN) and serum creatinine (SCr).

2.14 Statistical Analysis

Statistical analysis was performed with two-tailed unpaired Student's t-test between two groups. One-way analysis of variance (ANOVA) was performed for multiple groups, followed by Newman-Keuls test if $p < 0.05$. In all analysis, $p < 0.05$ was considered statistically significant and $p < 0.01$ was considered highly statistically significant.

3. Results and Discussion

3.1 Synthesis and Characterization of POEG-b-PVBIND Polymer

IND is a hydrophobic drug; however, it is difficult to be physically encapsulated into micelles[52–53]. Conjugating IND with PEG to generate a "PEGylated prodrug" increased solubility of IND by forming micellar solution. However, each prodrug molecule can only

carry one molecule of IND[54] and this prodrug is incapable of serving as a carrier for codelivery of other therapeutic agents. This has promoted us to design and synthesize an IND-based polymer with multiple units of IND moieties. We initially developed an IND-based polymer with a linear ethylene glycol vinyl ether linker that can carry 10 units of INDs (Figure S3). However, this carrier has limited capacity in formulating other hydrophobic agents (data not shown). Aromatic groups were then introduced into this system to increase loading capacity of co-delivered agents through **π-π** interaction[55–56]. To our best knowledge, this is the first IND-based nanocarrier that carries a number of INDs and, at the same time, is capable of codelivery of other hydrophobic agents (Figure S4).

The POEG-b-PVBIND polymer was obtained via several steps, as shown in Scheme 2. First, POEG macroCTA was synthesized by reversible addition-fragmentation transfer (RAFT) polymerization and the number of POEG units was calculated to be 17 (Figure S5). POEG macroCTA was then used to initiate the polymerization of vinylbenzyl chloride, yielding the amphiphilic POEG-b-PVB backbone. The number of repeated vinylbenzyl chloride units in the POEG-b-PVB backbone was calculated to be 10 based on the relative intensity ratio of the peaks at 6.0ppm-7.60ppm **(d)** and 3.35ppm **(a)** as shown in Figure 1A. The Boc-protected IND was synthesized (Figure S6) and conjugated to the POEG-b-PVB to afford POEG-b-PVBIND-Boc polymer. The Boc-groups of the as-synthesized POEG-b-PVBIND-Boc polymer were deprotected in TFA/DCM solution to afford the POEG-b-PVBIND polymer. The chemical structures of POEG-b-PVB, POEG-b-PVBIND-Boc and POEG-b-PVBIND polymers were confirmed by ^{1}H NMR (Figure 1). The peaks at 3.35ppm **(a)** and 3.70ppm **(b, c)** were attributed to the hydrophilic POEG block of the polymer. The successful conjugation of IND-Boc to the polymer backbone was confirmed by the appearance of IND peaks at 6.30ppm-7.60ppm **(e, f, g)** and the Boc peak at 1.45 ppm **(l)** as shown in Figure 1B. After deprotection, amine-bearing POEG-b-PVBIND polymer was obtained and de-protection of Boc group was confirmed by the disappearance of the peak at 1.45 ppm (Figure 1C). The number of IND per molecule of polymer was calculated to be 8. This indicated that the final ratio of benzyl chloride/IND after reaction was 5/4, suggesting that almost all the chloride groups in the polymer backbone were functionalized with IND. Also, IND loading content in the POEG-b-PVBIND polymeric prodrug carrier was calculated to be approximately14.8% (w/w).

3.2 Physicochemical Characterization of POEG-b-PVBIND and Dox-Loaded Micelles

POEG-b-PVBIND polymer is an amphiphilic molecule. The outermost nontoxic PEGylation reduces adsorption of the serum proteins by the nanoparticles in physiological environment and increases the solubility of IND by forming micelles in aqueous solution. The hydrophobic anti-tumor agent Dox can be entrapped into the core of POEG-b-PVBIND micelles through **π-π** stacking and hydrophobic interaction among Dox, aromatic linker and IND. The POEG-b-PVBIND micelles and POEG-b-PVBIND/Dox micelles were prepared through a dialysis method. As shown in Table 1 and Figure 2A, the prodrug polymer readily formed small-sized particles with an average hydrodynamic diameter of 17.90±0.45 nm and a polydispersity index of 0.0246±0.005. The zeta potential was −1.23±1.25 mv. Loading of Dox into the POEG-b-PVBIND micelles resulted in an increase in the particle size with an average hydrodynamic diameter of 50.83±1.25 nm and a polydispersity index of

0.015±0.007. The Dox Loading Efficiency (DLE) and Dox Loading Capacity (DLC) were 72.1% and 8.4%, respectively. Loading of Dox had no impact on the zeta potential of the particles (−2.34±2.48). Transmission electron microscopy (TEM) confirmed the homogeneously distributed spherical particles of POEG-b-PVBIND micelles and POEG-b-PVBIND/Dox micelles with no aggregation (Figure 2B). Based on their biophysical properties, our newly developed polymeric micelles are expected to efficiently and selectively accumulate in the solid tumor through EPR effect[57].

To examine the stability of POEG-b-PVBIND micelles upon dilution in blood stream, an important parameter for systemic delivery of particles to tumors, the critical micelle concentration (CMC) of POEG-b-PVBIND was determined using Nile red as a fluorescence probe. POEG-b-PVBIND micelles showed a low CMC of 0.00244 mg/ml, suggesting that they could maintain their stability after i.v. injection (Figure 2C). The colloidal stability of the micelles was further evaluated under 4 °C via following changes in sizes over time. POEG-b-PVBIND micelles alone could be stored at 4 °C for at least 60 days and Dox-loaded POEG-b-PVBIND micelle solution could be stored for at least 28 days without significant change in drug content and particle size, indicating their favorable stability in vitro[58] (Table 1).

The kinetic profile of Dox release from POEG-b-PVBIND/Dox was also tested. Free Dox was rapidly diffused across the dialysis bag with greater than 80% being diffused out of dialysis bag within 5h. In contrast, only 21% of Dox was detected outside the dialysis bag within 24h, indicating a good stability of POEG-b-PVBIND/Dox without burst drug release under physiological environment (Figure 3).

The release of IND from POEG-b-PVBIND in PBS followed a much slower kinetics and less than 5% of released IND was detected over 24h. However, the release of IND was accelerated following exposure to esterases (Figure S7). Nonetheless, only 15% of IND was released after 24 h, suggesting that IND was slowly released over a prolonged period of time following delivery to the tumors.

The cytotoxicity of free Dox, POEG-b-PVBIND micelles and POEG-b-PVBIND/Dox micelles against 4T1.2 cells was determined by MTT assay (Figure 2D). POEG-b-PVBIND micelles alone were not effective in inhibiting the proliferation of 4T1.2 tumor cells at our test concentrations while free Dox and Dox-loaded POEG-b-PVBIND micelles inhibited 4T1.2 cell proliferation in a concentration-dependent manner. Dox-loaded POEG-b-PVBIND micelles were less effective than free Dox, which is likely due to incomplete release of Dox over a short period of treatment as supported by the data from the release study (Figure 2C).

3.3 *In Vivo* Distribution of POEG-b-PVBIND Micelles

The tumor targeting efficiency of POEG-b-PVBIND micelles was investigated in a 4T1.2-bearing mouse model using DiR as a fluorescence probe[59]. First, the DiR-loaded POEG-b-PVBIND micelles were prepared and intravenously injected into the mice for in vivo imaging. The DiR-loaded POEG-b-PVBIND micelles were comparable to Dox-loaded POEG-b-PVBIND micelles in size (53.01 vs. 50.83 nm) (Figure S8). Figure 4A, 4B showed

that enhanced distribution of DiR-loaded POEG-b-PVBIND micelles was clearly observed at 12h and the fluorescence intensity continued to increase up to 36h post-injection. In contrast, free DiR was widely distributed in the mice with no obviously enhanced accumulation at the tumor sites at all time points examined

The accumulation of fluorescence in tumors and other major organs (heart, lung, liver, spleen and kidneys) was further examined by *ex vivo* imaging at 24 h postinjection. As shown in Figure 4C & 4D, the signals in normal organs were significantly higher or comparable to those in tumor tissues for free DiR. Particularly, high accumulation of free DiR was observed in the lung. As a quaternary ammonium salt, DiR carries a positive charge at the N atom under physiological pH. The effective accumulation in the lung is likely due to the interaction of the quaternary amine motif of DiR with the negatively charged cell membrane in the lung. Amine-containing basic compounds have been reported to be predominantly accumulated in the lung due to the effective binding to acidic phospholipids on the cell membrane, which is abundantly distributed in lung tissue[60–64]. In contrast, the signals of DiR-loaded POEG-b-PVBIND in tumor tissues were significantly higher than those in all normal organs examined, which was consistent with the data in Figure 4A. This indicates that the tumor-targeting ability of POEG-b-PVBIND micelles helps to reduce the distribution of their loaded agents in normal tissues, which shall help to reduce their toxicity in normal organs.

To examine whether POEG-b-PVBIND micelles can similarly deliver Dox to the tumors, the distribution of Dox in tumor tissues was examined by analyzing frozen tissue sections 24 h following injection of free Dox or Dox-loaded POEG-b-PVBIND micelles. As shown in Figure 5A, 5B, much more signals of Dox were found in tumor tissues treated with Dox-loaded POEG-b-PVBIND micelles compared to free Dox. It is also apparent that POEG-b-PVBIND and POEG-b-PVB were comparable in selective delivery of Dox to tumor tissues.

Taken together, the above data indicate that POEG-b-PVBIND micelles demonstrated effective passive targeting to tumors via EPR effect, which resulted in higher accumulation of Dox and IND in the tumor site. This might be attributed to the PEGylation on the surface of POEG-b-PVBIND micelles, which ensures a long circulation time for them to permeate into tumor sites. Meanwhile, the small size (~50 nm) of POEG-b-PVBIND micelles might also contribute to the effective accumulation at the tumor site[65–66].

3.4 *In Vivo* Therapeutic Efficacy

The antitumor efficacy of the IND prodrug-based nanocarrier was examined in an orthotopic syngeneic murine breast cancer model (4T1.2). BALB/c mice bearing tumors of 30 mm^3 in size were i.v. administered with saline, free Dox, POEG-b-PVBIND micelles, POEG-b-PVBIND/Dox, and POEG-b-PVB/Dox at a Dox does of 5mg/kg and an equivalent IND does of 20mg/kg on days 0, 3 and 6, respectively (Figure 6A). POEG-b-PVBIND micelles alone showed significant antitumor activity compared to the control mice that received only the saline treatment (Figure 6B, C), which might be attributed to the immune response activated by the released IND as shown later.

Free Dox only showed a modest effect in inhibiting the growth of 4T1.2 tumor. However, loading of Dox into POEG-b-PVBIND micelles led to a significant improvement in antitumor activity, much more effectively than either free Dox or POEG-b-PVBIND micelles alone. It is worth noting that POEG-b-PVBIND/Dox micelles were also more effective than POEG-b-PVB/Dox (Figure 6B, C). This is unlikely due to a more effective delivery of DOX by the POEG-b-PVBIND/Dox formulation as both formulations showed similar particle sizes (50.83 vs. 49.63 nm) (Figure S9) and they are comparable in the efficiency of delivery as shown by similar levels of Dox fluorescence intensity in tumors following delivery via POEG-b-PVB micelles or POEG-b-PVBIND micelles (Figure 5A, 5B). The observed activity of the POEG-b-PVBIND/DOX was likely attributed to both direct effect of chemotherapy on cancer cells and enhanced immuno-microenvironment from DOX/IND. In particular, the enhanced delivery of both DOX and IND through the POEG-b-PVBIND-based nanocarrier plays an important role in the enhanced antitumor activity.

We further examined the tumor histology at the end of drug treatment. As shown in Figure 6D (upper), H&E-stained tumor sections in the saline-treated group showed typical high density of tumor cells with large nuclei. However, the tumor sections in other treatments showed areas of necrosis. In addition, altered morphology of cancer cells with shrunk nuclei and cell damage was observed as well. Among all the five treatment groups, POEG-b-PVBIND/Dox micelles exhibited the most significant intra-tumor tissue damage.

We also performed immuno-histochemical (IHC) staining of Ki-67 protein to further evaluate the extent of tumor cell proliferation. As shown in Figure 6D (bottom) and Figure S10, POEG-b-PVBIND/Dox micelles-treated group exhibited the lowest level of Ki-67 expression, indicating significantly reduced tumor cell proliferation compared with other treatments. The results of histology and Ki-67 studies were consistent with those of tumor volume measurements.

3.4 Antitumor Immune Response *in Vivo*

To delineate a role of immune response in the POEG-b-PVBIND/DOX-mediated antitumor activity, the immune cell populations in the tumor tissues with various treatments were analyzed and compared by flow cytometry 10-days after various treatments. Figure 7A (i) shows that the total percentage of immune cells ($CD45^+$) was significantly increased in the tumors treated with POEG-b-PVBIND alone or POEG-b-PVBIND/Dox. The number of immune cells was also increased in the group treated with Dox alone or POEG-b-PVB/DOX although it was not statistically significant (Figure 7B (i)).

Figure 7A, 7B (ii) shows that the percentages of both $CD4^+$ T and $CD8^+$ T cells were significantly increased in the tumors treated with POEG-b-PVBIND micelles, alone or loaded with Dox. Treatment with free Dox or POEG-b-PVB/Dox micelles also led to a slight increase in the number of $CD8^+$ T cells. In contrast, the numbers of Treg cells were significantly decreased by all of the treatments, particularly POEG-b-PVBIND micelles alone or POEG-b-PVBIND/Dox micelles (Figure 7A, 7B (iii)). Accordingly, the ratios of CD8+ T cells/Treg cells were significantly increased in all of the treatments especially POEG-b-PVBIND micelles alone or POEG-b-PVBIND/Dox micelles (Figure 7B (iv)).

Figure 7C shows that free Dox was highly effective in increasing the number of functional CD8 cells (IFN-γ-producing $CD8^+$ T cells). Similar effects were observed for Dox loaded in POEG-b-PVB or POEG-b-PVBIND/Dox micelles. Treatment with POEG-b-PVBIND micelles alone led to a slight increase in the number of IFN-γ-producing $CD8^+$ T cells; however, it is not statistically significant.

MDSCs are highly immunosuppressive and play an important role in inhibiting the antitumor immunity[67]. Figure 7D shows that the number of MDSCs was significantly reduced in the tumor following treatment with POEG-b-PVBIND micelles alone. Treatment with POEG-b-PVBIND/Dox micelles also led to a significant decrease in the percentages of MDSCs, but less dramatically compared to the treatment by POEG-b-PVBIND micelle alone.

Overall, our results were consistent with the notion that Dox is a potent ICD drug and can induce antitumor immunity in addition to a direct killing effect on tumor cells. Our data also clearly showed that the IND prodrug-based carrier was highly effective in promoting an immuno-active tumor microenvironment. The significantly improved antitumor activity of POEG-b-PVBIND/Dox compared to other treatments is likely due to both the tumoricidal effect of Dox and a strong antitumor immune response that is potentiated by the IND following release from the POEG-b-PVBIND micelles.

3.5 Safety Evaluations

Figure 8A shows the changes in body weights of mice receiving different treatments throughout the therapy study. There were no significant differences in the body weights between control group and other treatment groups although mice receiving free Dox appeared to gain less weight. In addition, serum levels of aspartate transaminase (AST), alanine transaminase (ALT), alkaline phosphatase (ALP), and creatinine (SCr) were all within the normal ranges, suggesting minimal impact of the different treatments on the hepatic and renal functions (Figure 8B, 8C). Finally, no obvious changes in histology were found for all of the major organs examined including heart, liver, spleen, lung and kidney in mice receiving different treatments (Figure 8D). These data suggest the excellent safety of the POEG-b-PVBIND/Dox at a dose that demonstrated significant therapeutic efficacy.

4. Conclusions

We have developed a new, IND prodrug-based micellar system, POEG-b-PVBIND that can achieve codelivery of IDN and a hydrophobic chemotherapeutic agent such as Dox. Compared to our previous PEG-Fmoc-NLG919-based carrier, POEG-b-PVBIND allows incorporation of 8 units of immunostimulatory moieties instead of 1. POEG-b-PVBIND can realize controlled release of both conjugated drugs (IND) and encapsulated drugs (Dox). Dox was encapsulated in the hydrophobic core of micelles via hydrophobic interaction (intermolecular forces). IND was introduced into POEG-b-PVBIND micelles via a covalent bond (intramolecular forces). Intermolecular forces are weaker than intramolecular forces. Because of this, Dox has a much faster rate of release compared with that of IND. The relatively rapid release of Dox shall lead to the first round of anti-tumour response. In addition to direct effect on cancer cells, Dox also induces immune response due to enhanced

antigen presentation following killing of tumour cells (Figure 7B (ii), Figure 7C). Meanwhile, the slower release of active IND from the prodrug helps to sustain or enhance the magnitude of immune responses by reversing the suppressive immune microenvironment (Figure 7B, 7C, and 7D). The improved delivery together with the combination action between IND and DOX plays an important role in the enhanced overall antitumor activity (Figure 6B, C).

Supplementary Material

Refer to Web version on PubMed Central for supplementary material.

Acknowledgements

This work was supported in part by NIH grants R01CA174305, R01CA223788, and R01CA219399 (to Li).

References

1. Sharma P; Allison JP, The future of immune checkpoint therapy. Science 2015, 348 (6230), 56–61. [PubMed: 25838373]
2. Topalian SL; Drake CG; Pardoll DM, Immune checkpoint blockade: a common denominator approach to cancer therapy. Cancer cell 2015, 27 (4), 450–461. [PubMed: 25858804]
3. Brahmer J; Reckamp KL; Baas P; Crinò L; Eberhardt WE; Poddubskaya E; Antonia S; Pluzanski A; Vokes EE; Holgado E, Nivolumab versus docetaxel in advanced squamous-cell non–small-cell lung cancer. New England Journal of Medicine 2015, 373 (2), 123–135. [PubMed: 26028407]
4. Hodi FS; O'day SJ; McDermott DF; Weber RW; Sosman JA; Haanen JB; Gonzalez R; Robert C; Schadendorf D; Hassel JC, Improved survival with ipilimumab in patients with metastatic melanoma. New England Journal of Medicine 2010, 363 (8), 711–723. [PubMed: 20525992]
5. Munn DH; Mellor AL, IDO in the tumor microenvironment: inflammation, counter-regulation, and tolerance. Trends in immunology 2016, 37 (3), 193–207. [PubMed: 26839260]
6. Munn DH; Bronte V, Immune suppressive mechanisms in the tumor microenvironment. Curr Opin Immunol 2016, 39, 1–6. [PubMed: 26609943]
7. Prendergast GC; Malachowski WP; DuHadaway JB; Muller AJ, Discovery of IDO1 inhibitors: from bench to bedside. Cancer research 2017, 77 (24), 6795–6811. [PubMed: 29247038]
8. Lake RA; Robinson BW, Immunotherapy and chemotherapy—a practical partnership. Nature Reviews Cancer 2005, 5 (5), 397. [PubMed: 15864281]
9. Holmgaard RB; Zamarin D; Munn DH; Wolchok JD; Allison JP, Indoleamine 2, 3-dioxygenase is a critical resistance mechanism in antitumor T cell immunotherapy targeting CTLA-4. Journal of Experimental Medicine 2013, jem. 20130066.
10. Muller AJ; DuHadaway JB; Donover PS; Sutanto-Ward E; Prendergast GC, Inhibition of indoleamine 2, 3-dioxygenase, an immunoregulatory target of the cancer suppression gene Bin1, potentiates cancer chemotherapy. Nature medicine 2005, 11 (3), 312.
11. Gotwals P; Cameron S; Cipolletta D; Cremasco V; Crystal A; Hewes B; Mueller B; Quaratino S; Sabatos-Peyton C; Petruzzelli L; Engelman JA; Dranoff G, Prospects for combining targeted and conventional cancer therapy with immunotherapy. Nat Rev Cancer 2017, 17 (5), 286–301. [PubMed: 28338065]
12. Kroemer G; Galluzzi L; Kepp O; Zitvogel L, Immunogenic cell death in cancer therapy. Annu Rev Immunol 2013, 31, 51–72. [PubMed: 23157435]
13. Lake RA; Robinson BW, Immunotherapy and chemotherapy--a practical partnership. Nat Rev Cancer 2005, 5 (5), 397–405. [PubMed: 15864281]
14. Senkus E; Kyriakides S; Ohno S; Penault-Llorca F; Poortmans P; Rutgers E; Zackrisson S; Cardoso F; Committee EG, Primary breast cancer: ESMO Clinical Practice Guidelines for diagnosis, treatment and follow-up. Ann Oncol 2015, 26 Suppl 5, v8–30. [PubMed: 26314782]

15. Sun J; Sun L; Li J; Xu J; Wan Z; Ouyang Z; Liang L; Li S; Zeng D, A Multi-Functional Polymeric Carrier for Simultaneous Positron Emission Tomography Imaging and Combination Therapy. Acta biomaterialia 2018.

16. Sun J; Liu Y; Chen Y; Zhao W; Zhai Q; Rathod S; Huang Y; Tang S; Kwon YT; Fernandez C, Doxorubicin delivered by a redox-responsive dasatinib-containing polymeric prodrug carrier for combination therapy. Journal of Controlled Release 2017, 258, 43–55. [PubMed: 28501705]

17. Qu Y; Chu B; Shi K; Peng J; Qian Z, Recent progress in functional micellar carriers with intrinsic therapeutic activities for anticancer drug delivery. Journal of biomedical nanotechnology 2017, 13 (12), 1598–1618. [PubMed: 29490750]

18. Chen Y; Xia R; Huang Y; Zhao W; Li J; Zhang X; Wang P; Venkataramanan R; Fan J; Xie W, An immunostimulatory dual-functional nanocarrier that improves cancer immunochemotherapy. Nature communications 2016, 7, 13443.

19. Metz R; DuHadaway JB; Kamasani U; Laury-Kleintop L; Muller AJ; Prendergast GC, Novel tryptophan catabolic enzyme IDO2 is the preferred biochemical target of the antitumor indoleamine 2, 3-dioxygenase inhibitory compound D-1-methyl-tryptophan. Cancer research 2007, 67 (15), 7082–7087. [PubMed: 17671174]

20. Dolu i, E.; Larrieu P; Moineaux L; Stroobant V; Pilotte L; Colau D; Pochet L; Van den Eynde B. i.; Masereel B; Wouters J, Tryptophan 2, 3-dioxygenase (TDO) inhibitors. 3-(2-(pyridyl) ethenyl) indoles as potential anticancer immunomodulators. Journal of medicinal chemistry 2011, 54 (15), 5320–5334. [PubMed: 21726069]

21. Liu X; Shin N; Koblish HK; Yang G; Wang Q; Wang K; Leffet L; Hansbury MJ; Thomas B; Rupar M, Selective inhibition of indoleamine 2, 3-dioxygenase (IDO1) effectively regulates mediators of anti-tumor immunity. Blood 2010, blood-2009-09-246124.

22. Brincks E; Adams J; Essmann M; Turner B; Wang L; Ke J; Vahanian N; Link C Jr; Mautino M, Indoximod modulates AhR-driven transcription of genes that control immune function. Ratio 2018, 1, 0.25.

23. Chang MY; Smith C; DuHadaway JB; Pyle JR; Boulden J; Soler AP; Muller AJ; Laury-Kleintop LD; Prendergast GC, Cardiac and gastrointestinal liabilities caused by deficiency in the immune modulatory enzyme indoleamine 2, 3-dioxygenase. Cancer biology & therapy 2011, 12 (12), 1050–1058. [PubMed: 22157149]

24. 'Mac'Cheever MA, Twelve immunotherapy drugs that could cure cancers. Immunological reviews 2008, 222 (1), 357–368. [PubMed: 18364014]

25. Godin-Ethier J; Hanafi L-A; Piccirillo CA; Lapointe R, Indoleamine 2, 3-dioxygenase expression in human cancers: clinical and immunologic perspectives. Clinical cancer research 2011.

26. Metz R; Rust S; DuHadaway JB; Mautino MR; Munn DH; Vahanian NN; Link CJ; Prendergast GC, IDO inhibits a tryptophan sufficiency signal that stimulates mTOR: a novel IDO effector pathway targeted by D-1-methyl-tryptophan. Oncoimmunology 2012, 1 (9), 1460–1468. [PubMed: 23264892]

27. Prendergast GC; Malachowski WP; DuHadaway JB; Muller AJ, Discovery of IDO1 Inhibitors: From Bench to Bedside. Cancer Res 2017, 77 (24), 6795–6811. [PubMed: 29247038]

28. Prendergast GC; Smith C; Thomas S; Mandik-Nayak L; Laury-Kleintop L; Metz R; Muller AJ, Indoleamine 2, 3-dioxygenase pathways of pathogenic inflammation and immune escape in cancer. Cancer immunology, immunotherapy 2014, 63 (7), 721–735. [PubMed: 24711084]

29. Bahary N; Garrido-Laguna I; Cinar P; O'Rourke MA; Somer BG; Nyak-Kapoor A; Lee JS; Munn D; Kennedy EP; Vahanian NN, Phase 2 trial of the indoleamine 2, 3-dioxygenase pathway (IDO) inhibitor indoximod plus gemcitabine/nab-paclitaxel for the treatment of metastatic pancreas cancer: Interim analysis. American Society of Clinical Oncology: 2016.

30. Jackson E; Dees EC; Kauh JS; Harvey RD; Neuger A; Lush R; Antonia SJ; Minton SE; Ismail-Khan R; Han HS, A phase I study of indoximod in combination with docetaxel in metastatic solid tumors. American Society of Clinical Oncology: 2013.

31. Soliman HH; Minton SE; Han HS; Ismail-Khan R; Mahipal A; Janssen W; Streicher H; Vahanian NN; Link CJ; Ramsey WJ, A phase I study of Ad. p53 DC vaccine in combination with indoximod in metastatic solid tumors. American Society of Clinical Oncology: 2013.

32. Soliman HH; Minton SE; Ismail-Khan R; Han HS; Vahanian NN; Ramsey WJ; Kennedy E; Link CJ; Sullivan D; Antonia SJ, A phase 2 study of docetaxel in combination with indoximod in metastatic breast cancer. American Society of Clinical Oncology: 2014.
33. Zakharia Y; Johnson TS; Colman H; Vahanian NN; Link CJ; Kennedy E; Sadek RF; Kong FM; Vender J; Munn D, A phase I/II study of the combination of indoximod and temozolomide for adult patients with temozolomide-refractory primary malignant brain tumors. American Society of Clinical Oncology: 2014.
34. Zakharia Y; McWilliams R; Shaheen M; Grossman K; Drabick J; Milhem M; Rixie O; Khleif S; Lott R; Kennedy E, Abstract CT117: interim analysis of the phase 2 clinical trial of the IDO pathway inhibitor indoximod in combination with pembrolizumab for patients with advanced melanoma. AACR: 2017.
35. Calleja P; Irache J; Zandueta C; Martínez-Oharriz C; Espuelas S, A combination of nanosystems for the delivery of cancer chemoimmunotherapeutic combinations: 1-Methyltryptophan nanocrystals and paclitaxel nanoparticles. Pharmacological research 2017, 126, 77–83. [PubMed: 28893628]
36. Mautino MR; Kumar S; Zhuang H; Waldo J; Jaipuri F; Potturi H; Brincks E; Adams J; Marcinowicz A; Van Allen C, A novel prodrug of indoximod with enhanced pharmacokinetic properties. AACR: 2017.
37. Mautino M; Kumar S; Jaipuri F; Waldo J; Potturi H; Zhuang H, Salts and prodrugs of 1-methyl-d-tryptophan. Google Patents: 2017.
38. Lu J; Liu X; Liao Y-P; Salazar F; Sun B; Jiang W; Chang CH; Jiang J; Wang X; Wu AM, Nano-enabled pancreas cancer immunotherapy using immunogenic cell death and reversing immunosuppression. Nature communications 2017, 8 (1), 1811.
39. Yu S; Wang C; Yu J; Wang J; Lu Y; Zhang Y; Zhang X; Hu Q; Sun W; He C, Injectable Bioresponsive Gel Depot for Enhanced Immune Checkpoint Blockade. Advanced Materials 2018, 1801527.
40. Xu J; Sun J; Wang P; Ma X; Li S, Pendant HDAC inhibitor SAHA derivatised polymer as a novel prodrug micellar carrier for anticancer drugs. Journal of drug targeting 2018, 26 (5–6), 448–457. [PubMed: 29251528]
41. Song X; Wan Z; Chen T; Fu Y; Jiang K; Yi X; Ke H; Dong J; Yang L; Li L, Development of a multi-target peptide for potentiating chemotherapy by modulating tumor microenvironment. Biomaterials 2016, 108, 44–56. [PubMed: 27619239]
42. Huang Y; Liu Y; Liu Y; Song H; Wang Q, C ring may be dispensable for β-carboline: design, synthesis, and bioactivities evaluation of tryptophan analog derivatives based on the biosynthesis of β-carboline alkaloids. Bioorganic & medicinal chemistry 2016, 24 (3), 462–473. [PubMed: 26344597]
43. Yoo HS; Park TG, Biodegradable polymeric micelles composed of doxorubicin conjugated PLGA–PEG block copolymer. Journal of controlled Release 2001, 70 (1–2), 63–70. [PubMed: 11166408]
44. Duong HHP; Yung L-YL, Synergistic co-delivery of doxorubicin and paclitaxel using multi-functional micelles for cancer treatment. International journal of pharmaceutics 2013, 454 (1), 486–495. [PubMed: 23792465]
45. Lee ES; Na K; Bae YH, Doxorubicin loaded pH-sensitive polymeric micelles for reversal of resistant MCF-7 tumor. Journal of controlled release 2005, 103 (2), 405–418. [PubMed: 15763623]
46. Zhu J; Wang P; Shehu AI; Lu J; Bi H; Ma X, Identification of novel pathways in idelalisib metabolism and bioactivation. Chemical research in toxicology 2018, 31 (7), 548–555. [PubMed: 29896955]
47. Zhao J; Wan Z; Zhou C; Yang Q; Dong J; Song X; Gong T, Hyaluronic Acid Layer-By-Layer (LbL) Nanoparticles for Synergistic Chemo-Phototherapy. Pharmaceutical research 2018, 35 (10), 196. [PubMed: 30143878]
48. YANG Q; Tan T; Zhao J; Zhou C; Guo C; Wan Z; Song X; Gong T, A reversible decomposition approach for the formation of injectable, excipient-free, self-assembling nanocrystals. Chemical Communications 2019.

49. Yi X; Lian X; Dong J; Wan Z; Xia C; Song X; Fu Y; Gong T; Zhang Z, Co-delivery of pirarubicin and paclitaxel by human serum albumin nanoparticles to enhance antitumor effect and reduce systemic toxicity in breast cancers. Molecular pharmaceutics 2015, 12 (11), 4085–4098. [PubMed: 26422373]
50. Jiang K; Song X; Yang L; Li L; Wan Z; Sun X; Gong T; Lin Q; Zhang Z, Enhanced antitumor and anti-metastasis efficacy against aggressive breast cancer with a fibronectin-targeting liposomal doxorubicin. Journal of Controlled Release 2018, 271, 21–30. [PubMed: 29277681]
51. Song X; Liu H; Yang Q; Wan Z; Jiang K; Dong J; Jin Y; Fu Y; Sun X; Gong T, A Submicron Emulsion for Intravenous Injection of 7-Ethyl-10-Hydroxycamptothecin: Characterization, Pharmacolcinetic and Biodistribution Studies, In Vitro and In Vivo Antitumor Effect. LATIN AMERICAN JOURNAL OF PHARMACY 2016, 35 (6), 1369–1377.
52. WAN Z TUNABLE IMMUNOSTIMULATORY NANOCARRIER FOR IMPROVING CANCER IMMUNOCHEMOTHERAPY. University of Pittsburgh, 2017.
53. Awuah SG; Zheng Y-R; Bruno PM; Hemann MT; Lippard SJ, A Pt (IV) pro-drug preferentially targets indoleamine-2, 3-dioxygenase, providing enhanced ovarian cancer immuno-chemotherapy. Journal of the American Chemical Society 2015, 137 (47), 14854–14857. [PubMed: 26561720]
54. Sun J; Chen Y; Li K; Huang Y; Fu X; Zhang X; Zhao W; Wei Y; Xu L; Zhang P, A prodrug micellar carrier assembled from polymers with pendant farnesyl thiosalicylic acid moieties for improved delivery of paclitaxel. Acta biomaterialia 2016, 43, 282–291. [PubMed: 27422196]
55. Shi Y; Elkhabaz A; Yousef Yengej F. A.; van den Dikkenberg J; Hennink WE; van Nostrum CF, π–π stacking induced enhanced molecular solubilization, singlet oxygen production, and retention of a photosensitizer loaded in thermosensitive polymeric micelles. Advanced healthcare materials 2014, 3 (12), 2023–2031. [PubMed: 25388924]
56. Shi Y; van Nostrum CF; Hennink WE, Interfacially Hydrazone cross-linked thermosensitive polymeric micelles for acid-triggered release of paclitaxel. ACS Biomaterials Science & Engineering 2015, 1 (6), 393–404.
57. Rosenblum D; Joshi N; Tao W; Karp JM; Peer D, Progress and challenges towards targeted delivery of cancer therapeutics. Nature communications 2018, 9 (1), 1410.
58. Huo M; Zhao Y; Satterlee AB; Wang Y; Xu Y; Huang L, Tumor-targeted delivery of sunitinib base enhances vaccine therapy for advanced melanoma by remodeling the tumor microenvironment. Journal of Controlled Release 2017, 245, 81–94. [PubMed: 27863995]
59. Zhou C; Guo C; Li W; Zhao J; Yang Q; Tan T; Wan Z; Dong J; Song X; Gong T, A novel honokiol liposome: formulation, pharmacokinetics, and antitumor studies. Drug development and industrial pharmacy 2018, 44 (12), 2005–2012. [PubMed: 30058387]
60. Pack DW; Hoffman AS; Pun S; Stayton PS, Design and development of polymers for gene delivery. Nature reviews Drug discovery 2005, 4 (7), 581. [PubMed: 16052241]
61. Patil ML; Zhang M; Minko T, Multifunctional triblock nanocarrier (PAMAM-PEG-PLL) for the efficient intracellular siRNA delivery and gene silencing. ACS nano 2011, 5 (3), 1877–1887. [PubMed: 21322531]
62. Murakami T; Yumoto R, Role of phosphatidylserine binding in tissue distribution of amine-containing basic compounds. Expert opinion on drug metabolism & toxicology 2011, 7 (3), 353–364. [PubMed: 21332386]
63. Chander A; Johnson RG; Reicherter J; Fisher AB, Lung lamellar bodies maintain an acidic internal pH. Journal of Biological Chemistry 1986, 261 (13), 6126–6131. [PubMed: 3700387]
64. Tan T; Wang H; Cao H; Zeng L; Wang Y; Wang Z; Wang J; Li J; Wang S; Zhang Z, Deep Tumor-Penetrated Nanocages Improve Accessibility to Cancer Stem Cells for Photothermal-Chemotherapy of Breast Cancer Metastasis. Advanced Science 2018, 5 (12), 1801012. [PubMed: 30581704]
65. Cui X; Sun Y; Shen M; Song K; Yin X; Di W; Duan Y, Enhanced Chemotherapeutic Efficacy of Paclitaxel Nanoparticles Co-delivered with MicroRNA-7 by Inhibiting Paclitaxel-Induced EGFR/ERK pathway Activation for Ovarian Cancer Therapy. ACS applied materials & interfaces 2018, 10 (9), 7821–7831. [PubMed: 29411964]

66. Feng B; Zhou F; Hou B; Wang D; Wang T; Fu Y; Ma Y; Yu H; Li Y, Binary Cooperative Prodrug Nanoparticles Improve Immunotherapy by Synergistically Modulating Immune Tumor Microenvironment. Advanced Materials 2018, 1803001.

67. Gabrilovich DI; Nagaraj S, Myeloid-derived suppressor cells as regulators of the immune system. Nature reviews immunology 2009, 9 (3), 162.

Statement of significance

Indoleamine 2,3-dioxygenase (IDO) is an enzyme that can induce immune suppressive microenvironment in tumors. As a well-studied IDO inhibitor, indoximod (IND) represents a promising agent for cancer immunotherapy and could be particularly useful in combination with other chemotherapeutic agents. However, three major problems hinder its application: (1) IND is barely soluble in water; (2) IND delivery efficiency is limited (3) simultaneous delivery of two agents into tumor site is still challenging. Currently, most reports largely focus on improving the pharmacokinetic profile of IND alone via different formulations such as IND prodrug and IND nanocrystal. However, there is limited information about IND based co-delivery systems, especially for delivering hydrophobic chemotherapeutic agents. Here, we developed a new dual-functional polymeric prodrug carrier modified with a number of pendent IND units (denoted as POEG-b-PVBIND). POEG-b-PVBIND shows immunostimulatory and antitumor activities by itself. More importantly, POEG-b-PVBIND polymer is able to self-assemble into nano-sized micelles that are highly effective in formulating and codelivering other hydrophobic agents including doxorubicin (Dox), sunitinib (Sun), and daunorubicin (Dau), which can elicit antitumor immunity via promoting immunogenic cell death (ICD). We have shown that our new combination therapy led to a significantly improved antitumor activity in an aggressive murine breast cancer model (4T1.2).

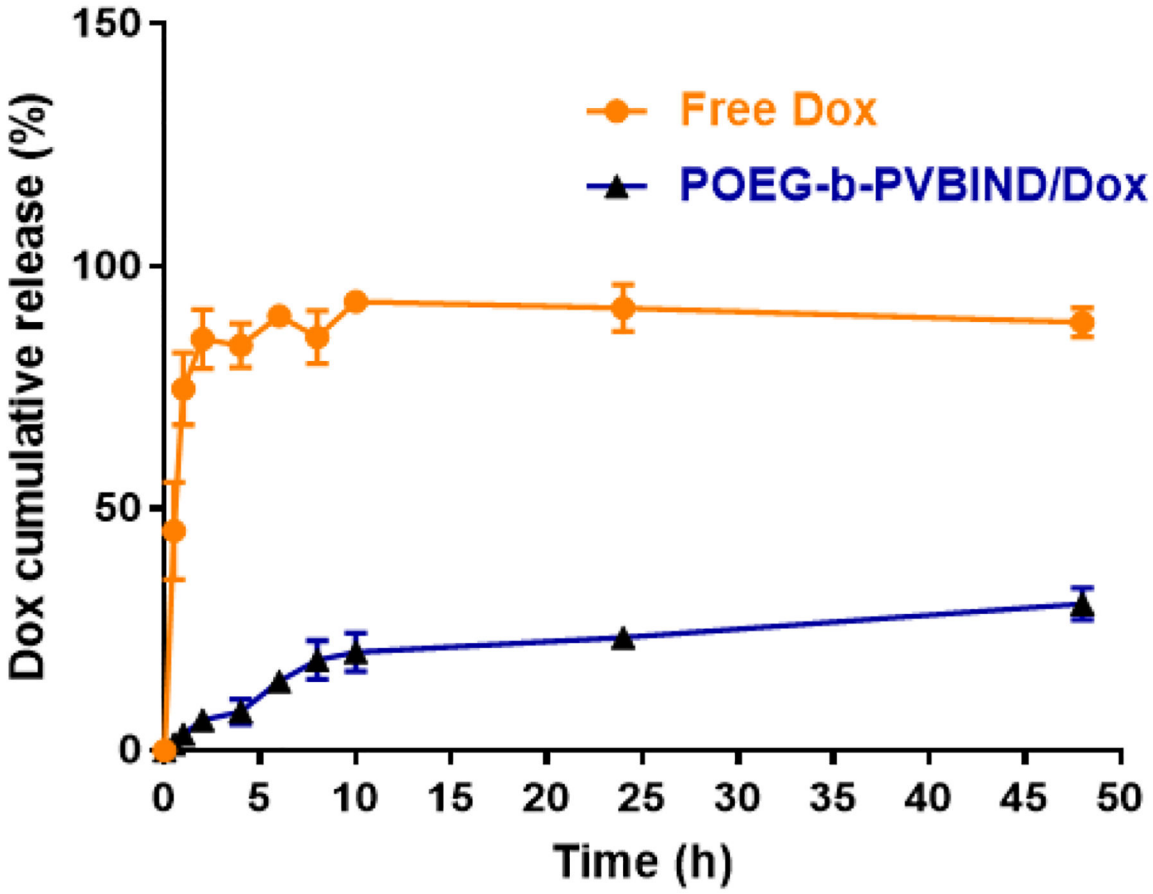

Figure 1 |.
^{1}H NMR spectrum of (A) POEG-b-PVB, (B) POEG-b-PVBIND-Boc, and (C) POEG-b-PVBIND polymers in DMSO.

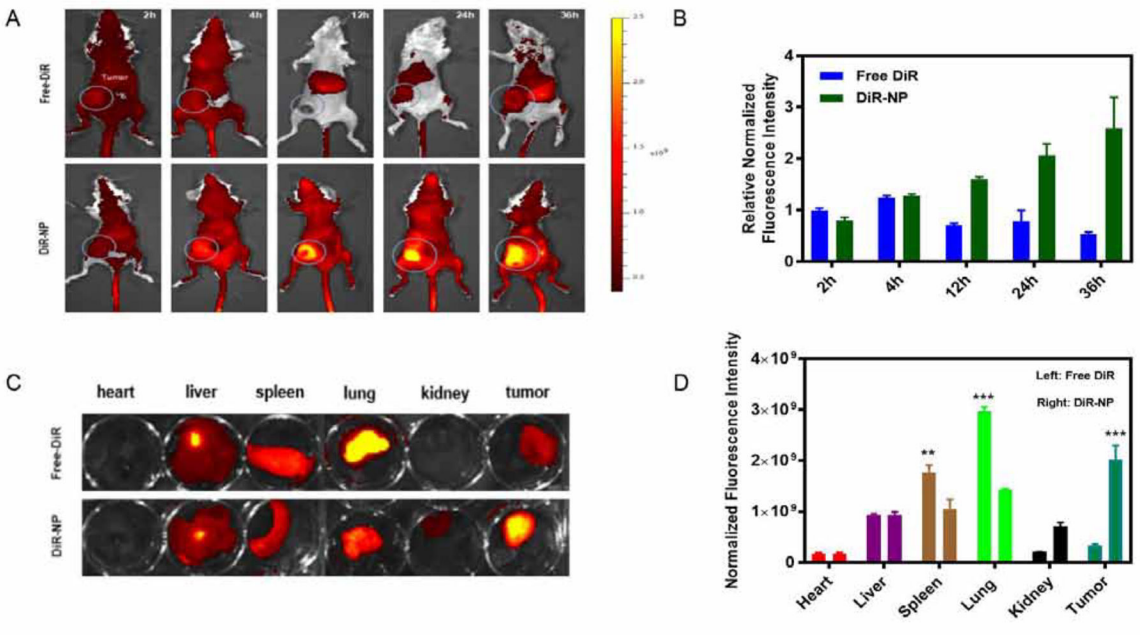

Figure 2 |. *In vitro* biophysical and biological characterizations of IND-based polymeric micelles.

(A) Size distribution and (B) TEM image of POEG-b-PVBIND micelles and POEG-b-PVBIND/Dox (carrier: drug, 35:1, w/w). Scale bar, 100nm; (C) Measurement of CMC of POEG-b-PVBIND micelles. (D) Cytotoxicity of POEG-b-PVBIND micelle, free Dox, and POEG-b-PVBIND/Dox against a mouse breast cancer cell line (4T1.2). Cells were treated for 72h and cytotoxicity was determined by MTT assay. Data are presented as means ± SD (n =5).

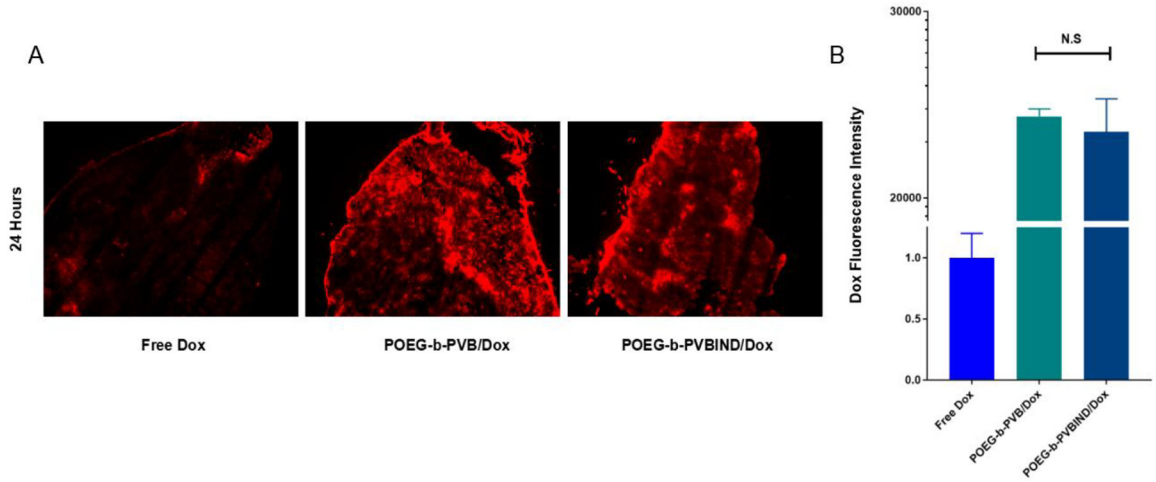

Figure 3 |.

DOX release profiles of DOX-loaded POEG-b-PVBIND micelles with free DOX as the control. PBS containing 0.5% (w/v) Tween 80 was used as the release medium. Data are presented as means ± SD (n =3).

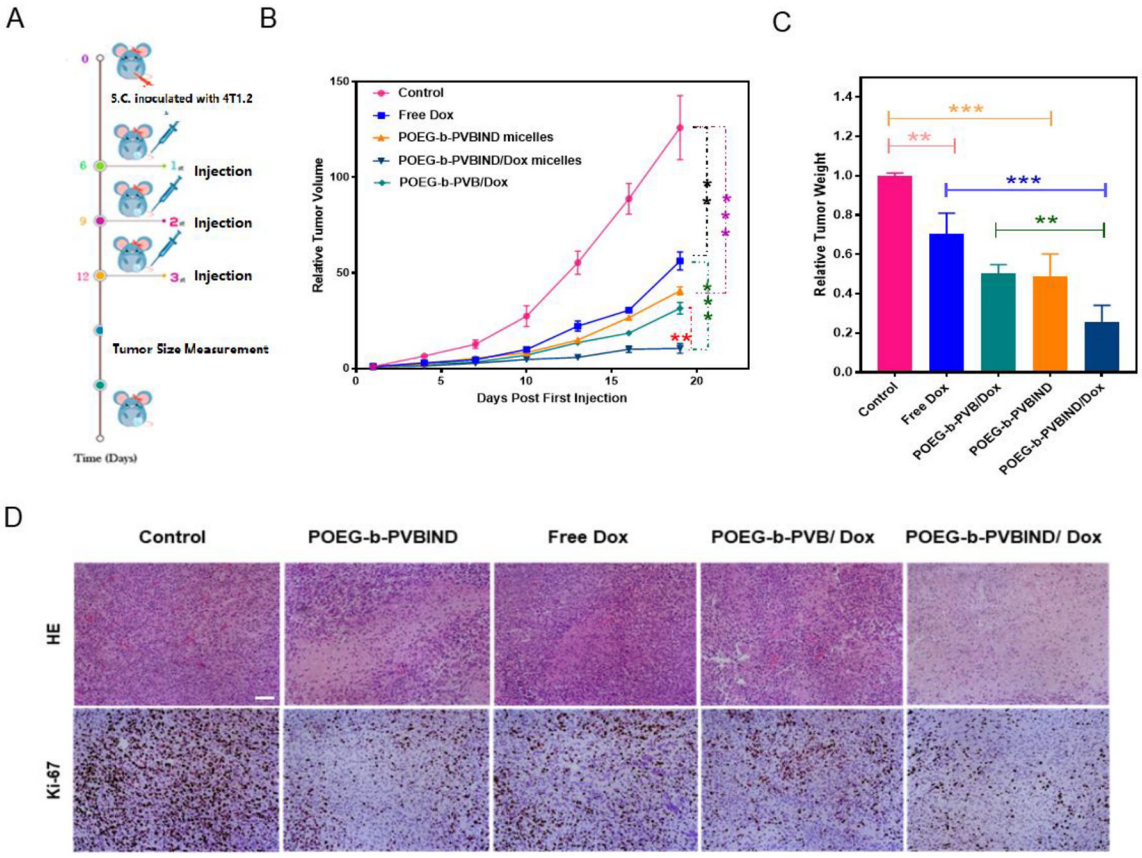

Figure 4 |. Tumor accumulation of NPs in a subcutaneous xenograft mouse model (4T1.2).

(A) Near-infrared images of mice at 2, 4, 12, 24, 36 h post-injection of free DiR and DiR-NP; (B) Fluorescence intensities of tumors at different time points (n=3, mean±SD); (C) Ex vivo fluorescence imaging of major organs and tumors 24 hours following injection of free DiR and DiR-NP; and (D) Relative normalized fluorescence intensity of major organs and tumors after 24 hours (n=3, mean±SD).

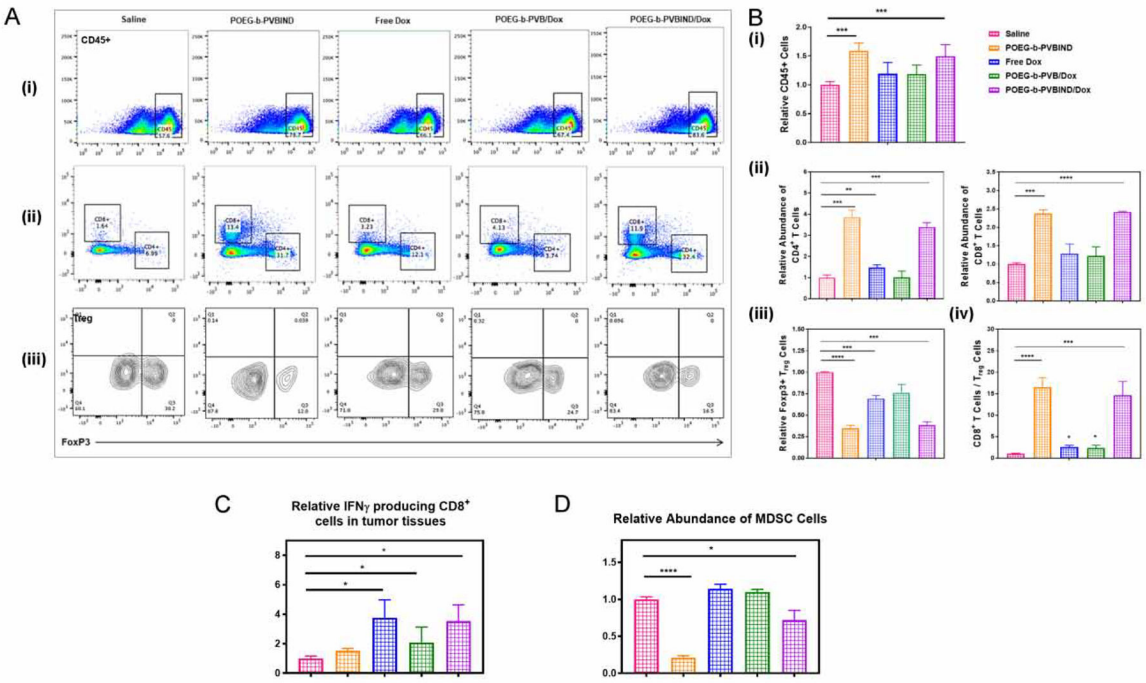

Figure 5 |.

(A) The distribution of Dox fluorescence in tumor tissues 24 hours following i.v. administration of free Dox, POEG-b-PVB/Dox or POEG-b-PVBIND/Dox (Magnification ×40, scale bar = 50 μm), the dose of Dox was 5 mg/kg; (B) Five randomly selected microscopic fields were quantitatively analyzed using image J, the results are displayed as mean ± S.D. (error bars).

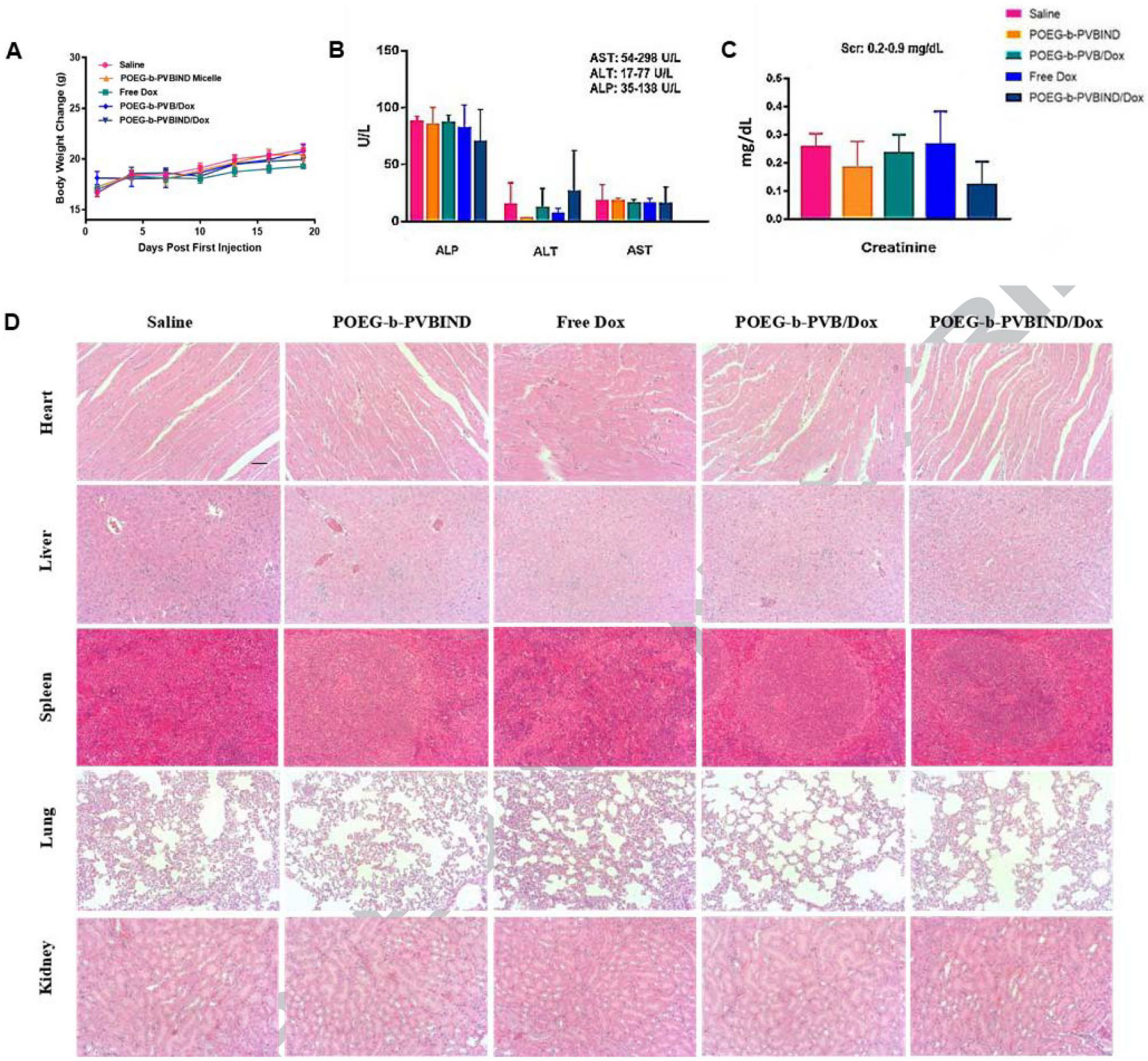

Figure 6 |. The evaluation of in vivo antitumor efficiency.

(A) Schematic representation of experimental design; (B) In vivo antitumor activity of various formulations in 4T1.2 tumor model. Dox dose was 5mg/kg and IND dose was 20mg/kg. Tumor sizes were plotted as relative tumor volumes; (C) Relative tumor weights at the end point (*P < 0.05; ** P < 0.01; *** P < 0.005, n=5); (D) Representative photomicrographs of tumors with H&E (upper) and Ki-67 immunohistochemical (bottom) staining (Magnification ×200, scale bar = 50 μm).

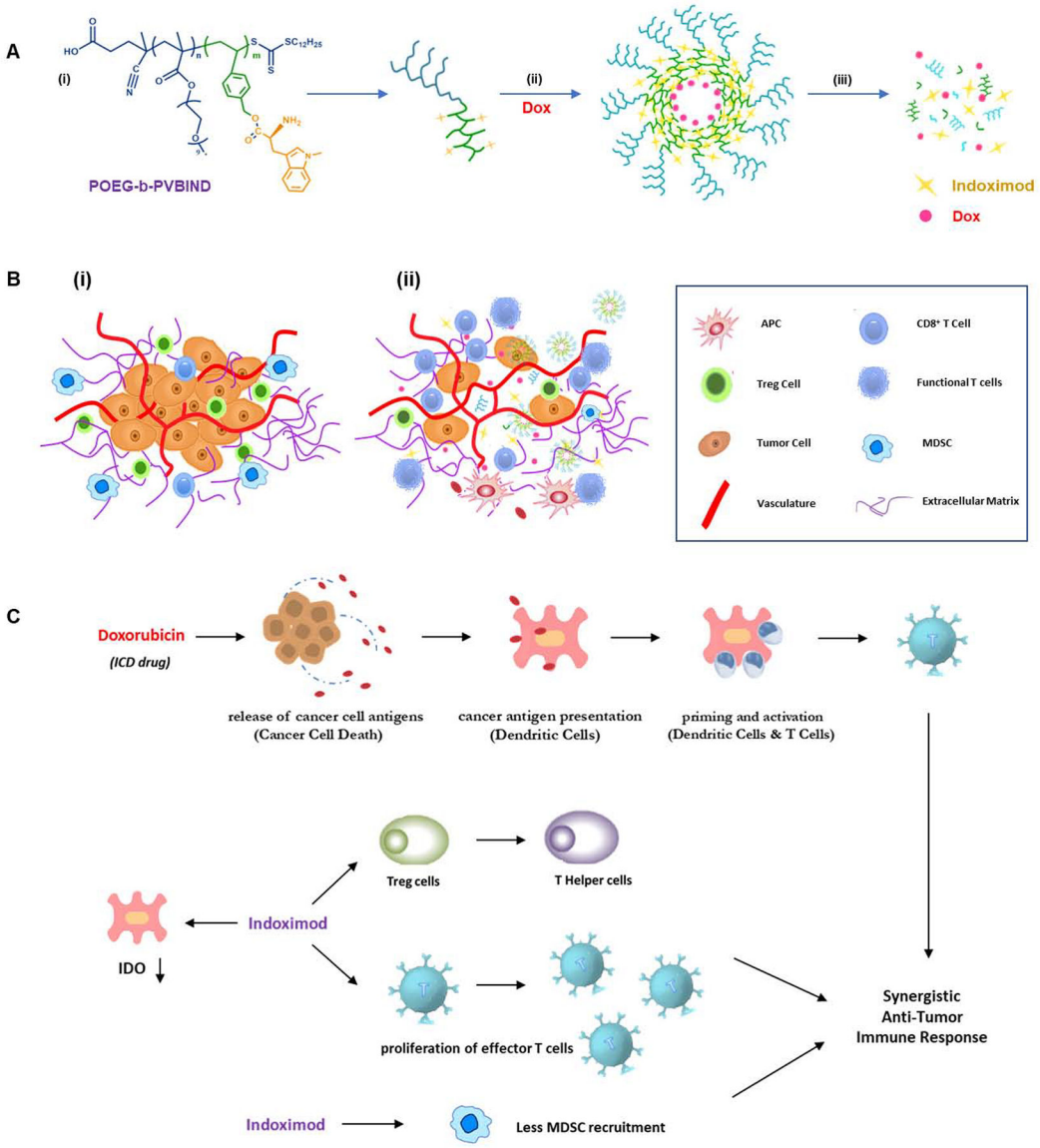

Figure 7 |. In vivo antitumor immune response after various treatments.

(A, B) Representative flow cytometric plots and percentages of $CD4^+$ T cells (ii) and $CD8^+$ T cells (ii) within the $CD45^+$ population (i); $FoxP3^+$ T regulatory cells within $CD4^+$ T cells (iii) in the tumor microenvironment; and ratios of $CD8^+$ T cells vs. T regulatory cells (iv). Percentages of (C) IFN-producing $CD8^+$ T cells, and (D) Myeloid-derived suppressor cells (MDSCs) in the tumor tissues. Data depict mean ± S.D., values were analyzed by two-tailed Student's t-test. (*P < 0.05; ** P < 0.01; *** P < 0.005)

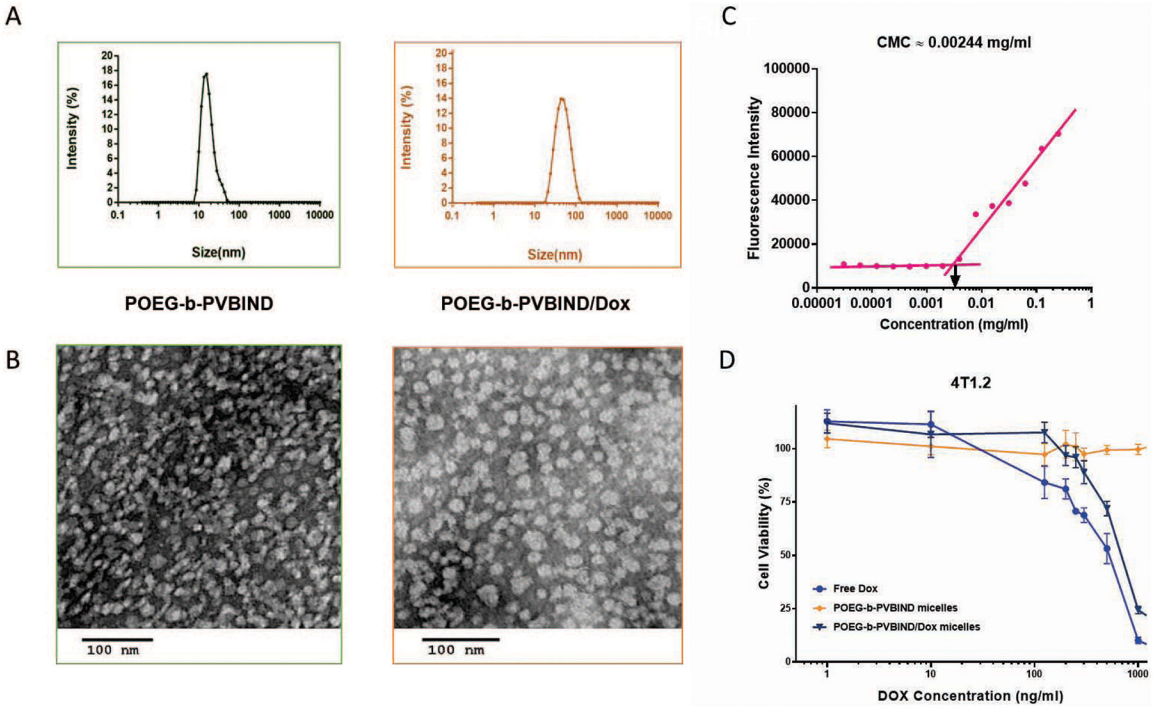

Figure 8 |. Safety evaluations.

(A) Body weight change (B) Liver and (C) Kidney function assays after various treatments. Results were expressed as the mean ± S.D. (n=5); The normal ranges for all the biochemical parameters are shown in the upper right corner of panels (B) and (C); (D) Representative photomicrographs of heart, liver, spleen, lung and kidney with H&E staining (Magnification ×200).

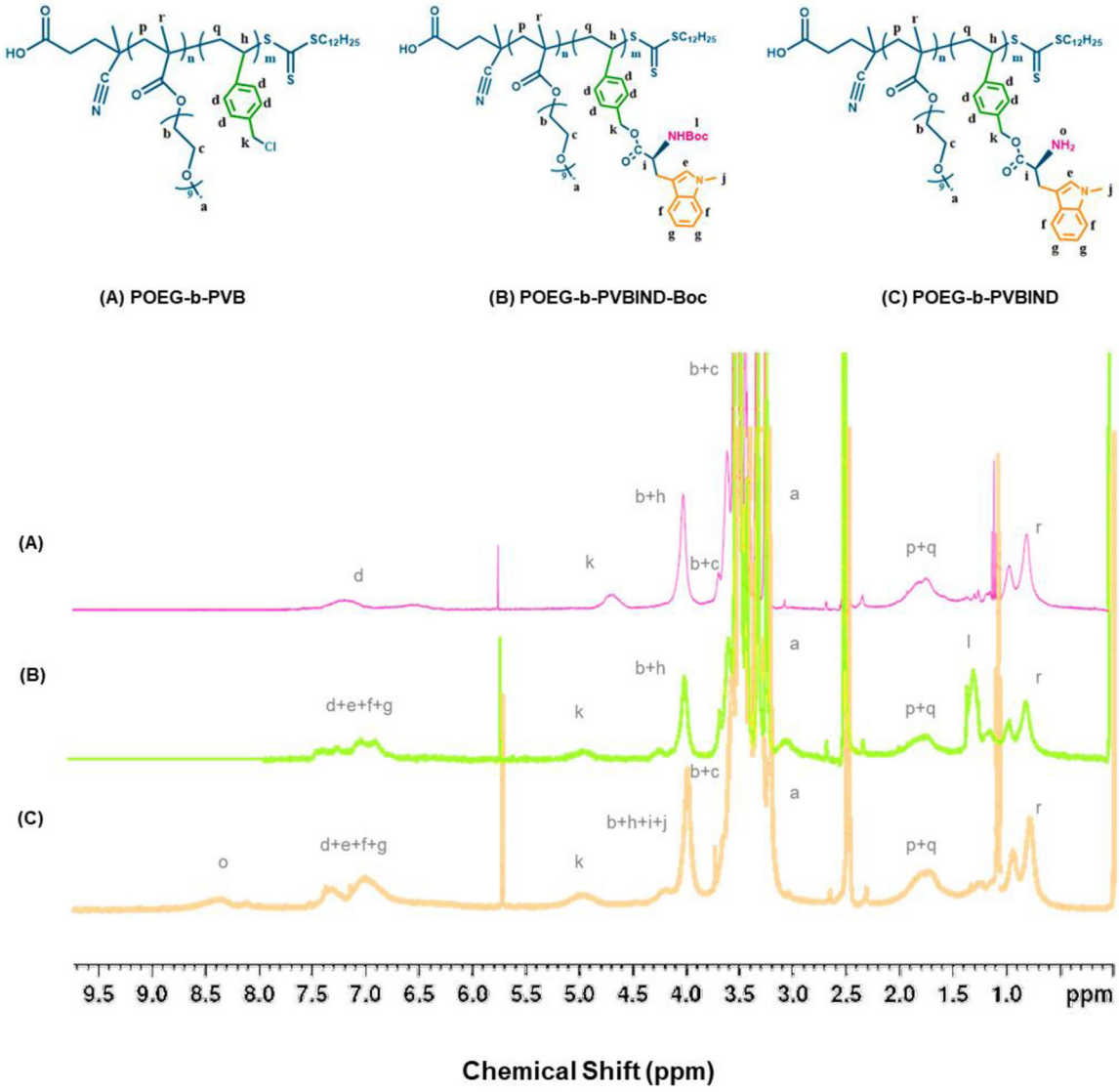

Scheme 1 |. IND-based polymeric micelles for immuno-chemotherapy

(A) illustration of encapsulation and release of IND and Dox from POEG-b-PVBIND/Dox micelles: (i) structure of POEG-b-PVBIND; (ii) self-assembly of Dox-loaded IND-based micelles; and (iii) dissociation of POEG-b-PVBIND/Dox micelles within tumor microenvironment; (B) Schematic diagram of POEG-b-PVBIND/Dox micelles to elicit anti-tumor immunity for improved chemoimmunotherapy: (i) initial immune-suppressive tumor microenvironment; (ii) immuno-active tumor microenvironment after treatment of POEG-b-PVBIND/Dox micelles; (C) Rationale of IND and Dox for synergistic immuno-chemotherapy.

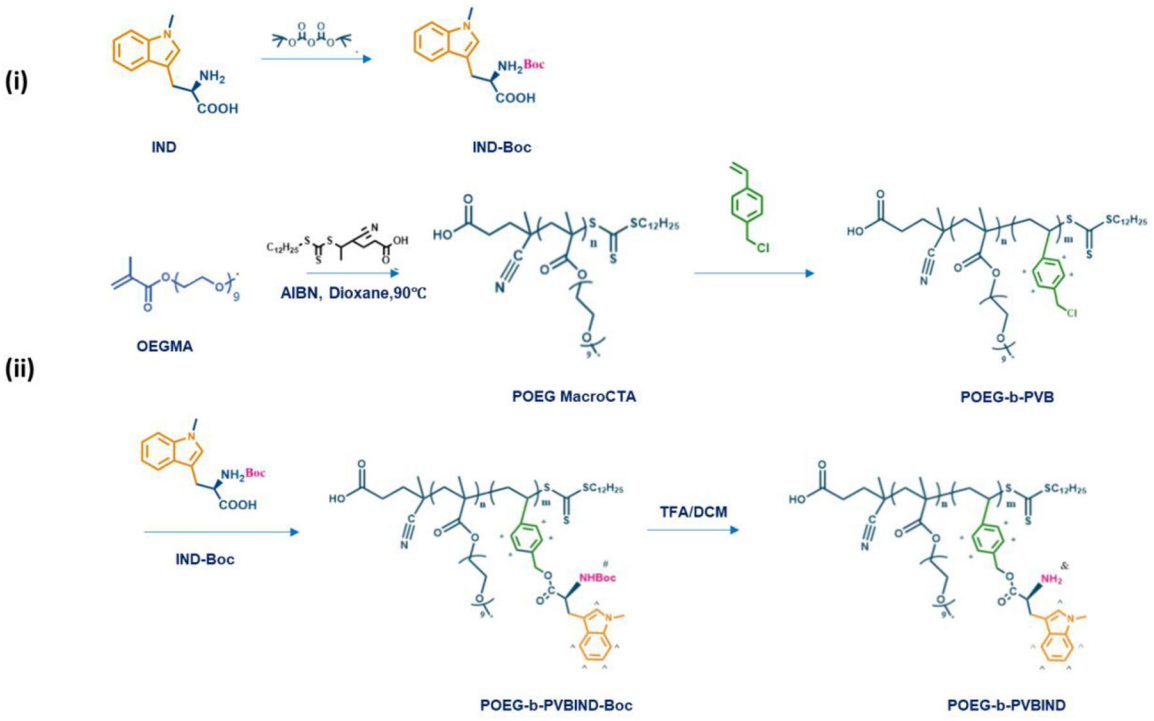

Scheme 2 |.
Synthesis of POEG-b-PVBIND polymer via RAFT polymerization and post-modification.

Table 1.

Biophysical Characterizations of blank and Dox-loaded POEG-b-PVBIND micelles.

Micelles	Size (nm)[a]	Zeta Potential (mv)[a]	PDI[a]	DLE (%)[b]	DLC (%)[c]	Stability[d]
POEG-b-PVBIND	17.90±0.45	−1.23±1.25	0.0246 ± 0.005	-----	-----	> 60 days
POEG-b-PVBIND / Dox	50.83±1.25	−2.34±2.48	0.015 ± 0.007	72.1	8.4	28 days

[a]Measured by dynamic light scattering particle sizer.

[b]DLE= DOX loading efficiency.

[c]DLC= DOX loading capacity.

[d]T=4 °C